



Dynamic modeling and analysis of a pouch type LiMn₂O₄/Carbon high power Li-polymer battery based on electrochemical-thermal principles

Meng Xiao, Song-Yul Choe*

Mechanical Engineering, 1418 Wiggins Hall, Auburn Univ., AL 36849, USA

HIGHLIGHTS

- Electrochemical and thermal model for Pouch type Li-polymer battery.
- Can show current/voltage/temperature distribution in pouch type cell.
- Terminal voltage, current and temperature distribution validation.

ARTICLE INFO

Article history:

Received 17 May 2012

Accepted 24 May 2012

Available online 13 July 2012

Keywords:

Pouch type Li-polymer battery
Electrochemical and thermal model
Dynamics
Temperature and current distributions

ABSTRACT

A dynamic model for a pouch type Li-polymer battery based on electrochemical and thermal principles is developed to analyze static and dynamic performances of a single cell. The model for the single cell is a quasi-three-dimensional, constructed by connecting one-dimensional models for micro cells using current collectors. The developed model can represent distributions of temperature, potentials, and current flows along with distribution of lithium ions through the plane. The model is coded using MATLAB and validated against a LiMn₂O₄/Carbon pouch type power cell. The static analysis includes responses of the terminal voltage at different current rates derived from the distribution of overpotentials in the micro cell as function of state of charge (SOC) as well as distribution of potentials and current flows in the single cell. Ion concentration in the electrodes and electrolyte of the micro cell are analyzed. The dynamic analysis includes voltage and temperature responses during charging and discharging processes. The results demonstrate effects of operation conditions on key variables of the cell performance that includes distribution of ions in the electrodes and electrolyte in micro cells as well as distribution of heat generation in single cell level during a charging and discharging process.

© 2012 Elsevier B.V. All rights reserved.

1. Introduction

Energy efficiency of future power systems can be substantially improved using energy storage that can capture energy and retrieve energy that is otherwise dissipated. Batteries are the most preferred energy storage because of high columbic efficiency, high energy and power density. Among different batteries technologies, Li-polymer battery is mostly preferred because of its highest power and energy density, and its drastic price drop that was triggered by the rapidly growing electronic market. The mass production of cells for the consumer electronics ensures a high production volume with increased quality. On the other hand, new applications such as electric and hybrid vehicles require increased power and energy density that is accomplished by employing a large size of active

areas by means of wrapping or folding electrodes, electrolytes, and separators together. Dependent upon the way of packaging, the cells can be manufactured into three different types, cylindrical, prismatic, or pouch type. Compared with the cells used for consumer electronics, these high power cells can be quickly degraded and performances might drop fast and becomes unstable because of high ion transport and gradient of ion concentrations and the associated high heat generation in conjunction with varying environmental operating conditions. The working mechanism of a cell is very complex and hard to understand in details, which presents one of technical barriers that prevents from optimal design of a cell and systems.

Terminal behavior of a battery cell can be described in three different ways, using empirical equations, equivalent circuit components, or electrochemical-thermal principles. The first two approaches are able to describe terminal behaviors, but ignore detailed physical effects that include spacious distribution of charging and discharging ionic and electronic current and the

* Corresponding author. Tel.: +1 334 844 3329; fax: +1 334 844 3307.

E-mail addresses: mzx0001@auburn.edu, xiaomeng996@sohu.com (M. Xiao), choe@auburn.edu (S.-Y. Choe).

Nomenclature	
<i>a</i>	Specific surface area for electrode (cm ⁻¹)
<i>c</i>	Concentration (mol L ⁻¹)
<i>D</i>	Diffusion coefficient (cm ² s ⁻¹)
<i>E</i>	Energy storage (J)
<i>F</i>	Faraday constant (96,487 C mol ⁻¹)
<i>e</i>	Energy storage density (J cm ⁻¹)
<i>i₀</i>	Reference exchange current density (A cm ⁻²)
<i>j</i>	Transfer current density (A cm ⁻²)
SOC	State of charge
<i>n</i>	Amount of active electrode material
<i>R</i>	Universal gas constant (8.3143 J mol ⁻¹ K ⁻¹)
<i>T</i>	Cell temperature (K)
<i>U</i>	Standard potential affected by solid concentration (V)
<i>x</i>	Stoichiometric number in negative electrode or coordinate
<i>y</i>	Stoichiometric number in positive electrode or coordinate
<i>W</i>	Work (J)
<i>t₀⁺</i>	Initial transference number
Greek symbols	
ϵ	Porosity of a porous medium
ϕ	Potential in a phase (V)
η	Surface overpotential (V)
κ	Ionic conductivity of electrolyte (S cm ⁻¹)
κ_D	Diffusion conductivity (A cm ⁻¹)
ρ	Density (g cm ⁻³)
σ	Conductivity of solid active material (S cm ⁻¹)
Subscripts	
<i>a</i>	Anode reaction
<i>c</i>	Cathode reaction
<i>e</i>	Electrolyte phase
eff	Effective
<i>s</i>	Solid phase

associated temperature rise at different state of charge (SOC). In addition, operating conditions like cycling, ambient temperature, and storage times cannot be considered. By contrast, the model based on electrochemical-thermal principles can better represent those major effects, but parameters necessary for the model are difficult to characterize and obtain. The electrochemical model known as a thin-film model was proposed by M. Doyle, T. Fuller, and J. Newman [1]. The model was extended by reflecting other cathode materials like LiCoO₂, LiMn₂O₄ [2] and LiFePO₄ [3]. Later, performance of cells for a mixture of two different active materials in electrodes, Li_yNi_{0.80}Co_{0.15}Al_{0.05}O₂ and Li_yMn₂O₄ was studied [4]. In addition, the model was used to investigate effects of material properties on performance, which include transference number [5], activity coefficient in electrolyte [6], diffusion coefficient in LiPF₆ electrolyte [7], and particle size distributions on the discharge capacity [8]. Furthermore, the model was improved by adding the energy equation [9] and the efficiency of batteries during cycling was investigated [10]. Effects of side reactions were also studied [11]. Other studies include relaxation phenomena of a lithium ion battery [12], current limitation on pulse operation [13], degradation of the battery in a pocket computer [14], calculation of heat transfer [15], and optimal design of a battery system used for electric vehicles [16]. However, the research work above has not extended to a high power pouch cell type lithium Polymer battery that is currently widely accepted for applications to electric vehicle (EV) and hybrid electric vehicle (HEV). Therefore, we developed a quasi-three-dimensional dynamic model based on the principles of electrochemical kinetics, mass balances, charge conservations and energy balance. The model is capable of representing ion transport, gradients of ion concentrations and two-dimensional distribution of potentials, current density and temperature as well as terminal voltage and current as a function of time.

2. Setup for development of a model for a single cell

A micro cell and a pouch type of a single cell are shown in Fig. 1, respectively. The single cell is assumed to be made of micro cells that are connected in parallel by current collectors of both electrodes.

Each of the micro cells is assumed to be a sandwiched model that is composed of a negative electrode, a separator, and a positive electrode. The materials are porous and equally mixed with electrolyte materials. In addition, particles dispersed at the cathode and

anode electrodes have a same radius, r_s , and are in contact with neighboring particles. The working mechanism of the micro cell is described using five variables that present concentrations in electrodes and electrolyte, potentials in solid and electrolyte, and overpotentials under isothermal condition. Since the conductivity of current collectors is relatively high, it is assumed that no lateral current flows from one micro cell to another, so all lateral effects can be ignored. In addition, the current collectors on each layer have the same potential, so that only two current collectors are considered for the model. The micro cell becomes a one-dimensional model. The tab current of the two collectors in the model are obtained by dividing total tab current by the number of layers.

The number of micro cells is equal to that of the grids, given by meshing the single cell. The number of grids in the following calculation is 1900, resulting from 38 divisions in the *x*-direction (*x* = 38) and 50 divisions in the *y*-direction (*y* = 50). The area of each individual micro cell may be obtained by dividing the cell area by the number of grids.

When ions and electrons are transported through electrolyte and external circuit, chemical reactions will take place at the surface of the electrode particles that contact electrolyte. After the reactions have been completed, the free ions are located in electrodes and diffuse until intercalated. The electrodes are approximated with spheres and it is assumed that the lithium ions diffuse only in the radial direction, driven by the gradient of the Li-ion concentration.

A schematic diagram for the model of a single cell is shown in Fig. 2, where initial conditions, input variables and parameters for the model, and outputs are included. The parameters used for the model are appended. The input variables are electric loads that can be bi-directional current and voltage as a function of time, while the outputs are responses of the loads in terminal voltage or current, SOC, and temperature distributions as well as other internal variables. In addition, the diagram shows how governing equations of the micro cells are connected each other and with those in the single cell.

3. Governing equations

3.1. Overpotentials

Current generated by chemical reactions are described by the Butler–Volmer equations, shown in Eq. (1).

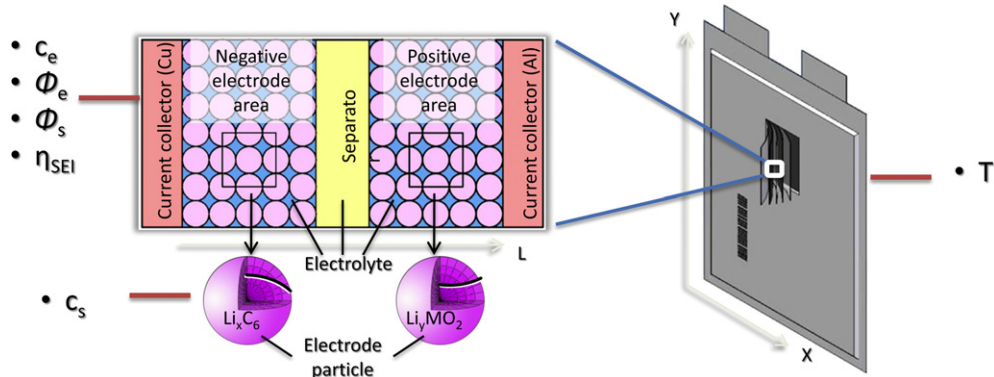


Fig. 1. A micro cell and a pouch type single cell.

$$j^{\text{Li}} = a_s \cdot i_0 \left(\exp\left(\frac{\alpha_a \cdot n \cdot F}{R \cdot T} (\eta - \eta_{\text{SEI}})\right) - \exp\left(-\frac{\alpha_c \cdot n \cdot F}{R \cdot T} (\eta - \eta_{\text{SEI}})\right) \right), \quad (1)$$

$$\eta = \phi_s - \phi_e - U$$

where j^{Li} is the current density, i_0 is the exchange current density, a_s is the specific interfacial surface area, ϕ_s is the solid potential, ϕ_e is the electrolyte potential, U is the equilibrium potential, T is the absolute temperature, n is the number of electrons involved in the electrode reaction, F is the Faraday constant and R is the universal gas constant. α is the symmetry factor that is dimensionless and presents a ratio between oxidation and reduction. η_{SEI} is the additional overpotential caused by the Solid Electrolyte Interphase (SEI) layer.

The exchange current density, i_0 , is the intrinsic rates of electrons and ions transfer at the interface between electrolyte and electrodes. It can be expressed with concentrations and symmetric factors, α_a and α_c , that describe bi-directions of one reversible semi-reaction.

$$i_0 = k(c_{s,\text{max}} - c_s)^{\alpha_a} c_s^{\alpha_c} c_e^{\alpha_c} \quad (2)$$

where c_s and c_e refer to the lithium ion concentration in solid and electrolyte and $c_{s,\text{max}}$ is the theoretical maximum ion concentration in solid. α_a and α_c is the oxidation and reduction symmetry factor.

3.2. Charge conservations, ions transport, and mass balance

The charges produced in oxidation processes should be the same as those consumed in the reduction process. This relationship is described using Ohm's law, expressed as a function of current and potential gradients. Ion transport in the electrolyte is governed by the Nernst–Planck equation, where migration and diffusion terms are considered, as shown in the following equation.

$$\frac{\partial}{\partial x} \left(\kappa_{\text{e}}^{\text{eff}} \cdot \frac{\partial \phi_e}{\partial x} \right) + \frac{\partial}{\partial x} \left(\kappa_{\text{D,e}}^{\text{eff}} \cdot \frac{\partial}{\partial x} (\ln c_e) \right) + j^{\text{Li}} = 0 \quad (3)$$

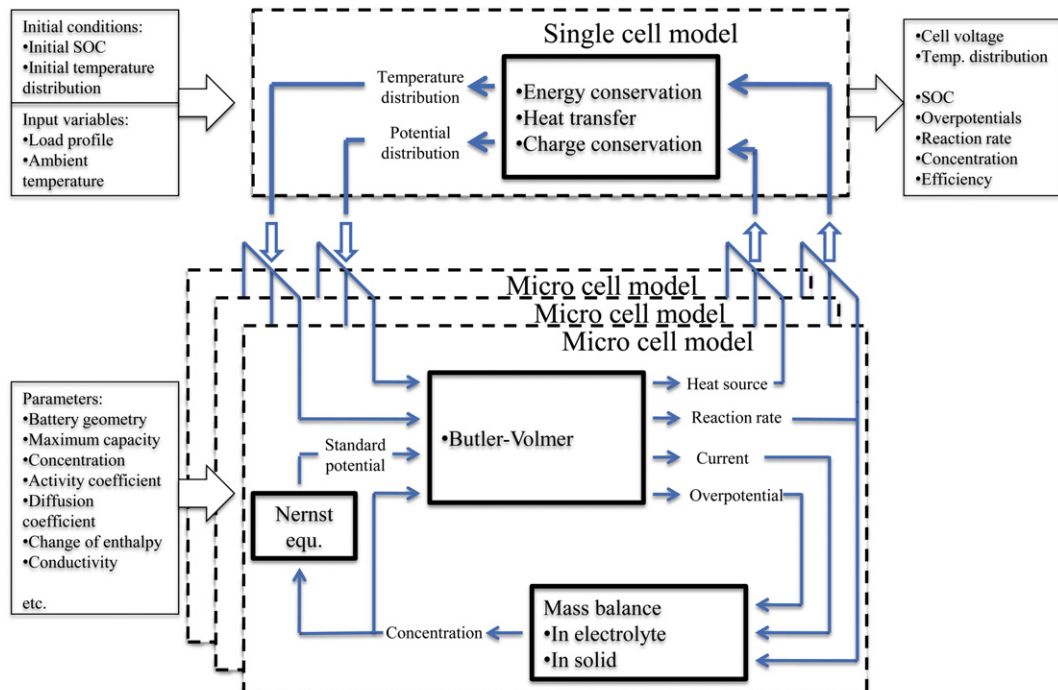


Fig. 2. Scheme of the model.

where j^{Li} is the current density in the electrolyte or solid phase, ϕ_e is the electrolyte potential, c_e is the concentration of the electrolyte, κ_e^{eff} is the effective electrolyte conductivity, while κ_D^{eff} is the concentration driven diffusion conductivity.

As for charge transport in solid, no diffusion term is necessary for electron transport in solid because it is solely governed by Ohm's law.

$$\frac{\partial}{\partial x} \left(\sigma^{\text{eff}} \cdot \frac{\partial}{\partial x} \phi_s \right) = j^{\text{Li}} \quad (4)$$

where σ^{eff} is the solid phase electronic conductivity.

3.3. Material balance

Charges produced or consumed by chemical reactions taking place in the electrodes are conserved. The chemical process in the entire cell can be described using a material balance principle. Hence, the balance of materials in electrolyte is affected by the gradient of ion concentrations. Since the electrode pores are filled with electrolyte, the balance should consider the porosity of the material. Therefore, the diffusion coefficient is redefined by considering the porosity as follows:

$$D_e^{\text{eff}} = D_e \cdot \varepsilon_e^p \quad (5)$$

where the diffusion coefficient, D_e , is constant. The material balance equation for the electrolyte considering the porosity is as follows:

$$\frac{\partial(\varepsilon_e c_e)}{\partial t} = \frac{\partial}{\partial x} \left(D_e^{\text{eff}} \cdot \frac{\partial}{\partial x} c_e \right) + \frac{1 - t_+^0}{F} j^{\text{Li}} = 0 \quad (6)$$

where c_e is the concentration of lithium ion in electrolyte, F is the Faraday constant, t_+^0 is the initial transference number, ε_e is the porosity, and j^{Li} is the current density [17].

For electrodes,

$$\frac{\partial c_s}{\partial t} = \frac{D_s}{r^2} \frac{\partial}{\partial r} \left(r^2 \frac{\partial c_s}{\partial r} \right) \quad (7)$$

where c_s is the lithium ion concentration in electrode and r is the radius of an electrode particle.

When reaction rates change, the current density varies accordingly. Consequently, the concentration is changed.

The reaction rate, j^{Li} , determined by the Butler–Volmer equation is the most important variable that affects not only the charge conservation equations but also the mass transport equation.

3.4. Energy conservation

Temperature in operating cells affects the performance and degradation of materials, which is described using the energy equation:

$$\rho C_p \frac{\partial T}{\partial t} = \frac{\partial}{\partial x} \left(k_x \frac{\partial T}{\partial x} \right) + \frac{\partial}{\partial y} \left(k_y \frac{\partial T}{\partial y} \right) + \frac{\partial}{\partial z} \left(k_z \frac{\partial T}{\partial z} \right) + Q + Q_{\text{convec.}} \quad (8)$$

where ρ , C_p , k and Q are the density, heat capacity, thermal conductivity, and heat-generation rate per unit volume, respectively.

The heat source term below in Eq. (9), Q , is generally used to calculate the temperature [18].

$$Q = I \left(U_{\text{OCV}} - V_t - T \cdot \frac{\partial U_{\text{OCV}}}{\partial T} \right) \quad (9)$$

The equation indicates that no heat will be generated when the current goes zero. In reality, heat is continuously generated by the

currents that are caused by the non-uniformity of electrochemical energy state gradients, which is called the heat of mixing. Therefore, the heat source term, Q , is divided into three terms, a reversible heat in micro cell (q_{rev}), an irreversible heat in micro cell (q_{irr}), and the Joule heating caused by the current collectors (q_{cc}) in a single cell per unit volume.

$$Q = \int_V q_{\text{rev}} dV + \int_V q_{\text{irr}} dV + \int_V q_{\text{cc}} dV \quad (10)$$

The reversible heat is a result of the change of entropy during a chemical reaction ($T\Delta S$). The rate of the heat generated per volume can be expressed as follows:

$$q_{\text{rev}} = j^{\text{Li}} \cdot T \cdot \frac{\partial E}{\partial T} \quad (11)$$

For calculation of irreversible heat generation, a following modification is suggested. When a battery is charged, electric energy supplied to the cell at the terminal is equal to a sum of electrochemical energy stored in the battery and irreversible heat dissipated. When discharged, the electric energy obtained at the terminal is the difference between the electrochemical energy and the irreversible heat. When the charging current is very low, it can be assumed that the energy dissipated is negligible. Then, the electrochemical energy can be expressed as follows:

$$\begin{aligned} E_{\text{chem}}(\text{SOC}) &= Q_{\text{max}} \int_{\text{SOC}_0}^{\text{SOC}} U_{\text{OCV}} \cdot d\text{SOC} \\ &= Q_{\text{max}} \int_{\text{SOC}_0}^{\text{SOC}} (U_+^{\text{equ}} - U_-^{\text{equ}}) \cdot d\text{SOC} \end{aligned} \quad (12)$$

Since there are always gradients of lithium ion concentrations, equilibrium potentials and current density, total amount of the electrochemical energy can be obtained by integrating the energy in a small control volume. On the other hand, change of SOC is proportional to change of concentration in a volume, so the SOC in the equation above can be substituted by C_s as follows:

$$E_{\text{chemical}} = -\varepsilon_s \cdot F \cdot \int_V C_{s+} \cdot U_+^{\text{equ}} \cdot dV - \varepsilon_s \cdot F \cdot \int_V C_{s-} \cdot U_-^{\text{equ}} \cdot dV \quad (13)$$

where ε_s is the active material volume fraction, F is the Faraday constant, c_s is the solid phase lithium ion concentration and U_{equ} is the equilibrium potential.

The irreversible heat generation rate for a micro cell is the difference between the electrical power supplied to the cell ($-V_{\text{micro}} \cdot I_{\text{micro}}$) and the power ($P_{\text{chem.}}$) contributing to the chemical energy increase that is obtained by differentiating the electrochemical energy with respect to the time. When charging, $0 < P_{\text{chem.}} < -V_{\text{micro}} \cdot I_{\text{micro}}$ and when discharging, $P_{\text{chem.}} < -V_{\text{micro}} \cdot I_{\text{micro}} < 0$, so that q_{irr} always becomes positive.

$$q_{\text{irr}} = -V_{\text{micro}} \cdot I_{\text{micro}} - P_{\text{chemical}} \quad (14)$$

The heat generation rate caused by the Joule heating in the current collectors is as follows:

$$q_{\text{cc}} = \sigma \cdot (\nabla \phi_{\text{cc}})^2 \quad (15)$$

In addition, the heat transfer by convection is considered.

$$Q_{\text{convec.}} = h_C \cdot (T_s - T_{\infty}) \quad (16)$$

where h , T_s , and T_{∞} denote the convective heat transfer coefficient, the surface temperature, and ambient temperature, respectively.

3.5. Model simplifications

Terminal voltage of a micro cell is given as a difference between electrode potentials and equilibrium potential. The electrode potentials are a function of concentration given by the Nernst equation. The equilibrium potential of a cell is called open circuit voltage (OCV) when no current flows. The OCV is the difference between the two standard potentials of the positive and negative electrode and is measured experimentally. Separation of individual equilibrium potentials for positive and negative electrodes from the measured OCV are carried out using an empirical equation for the equilibrium potential in negative electrode given in [19].

$$U_-(x) = 8.00229 + 5.0647x - 12.578x^{1/2} - 8.6322e^{-4x^{-1}} + 2.1765e^{-5x^{3/2}} - 0.46016\exp(15(0.06-x)) - 0.55364\exp(-2.4326(x-0.92)) \quad (17)$$

Currents produced during chemical reactions are a function of overpotentials governed by the Butler–Volmer equation that consists of two exponential functions. In fact, the overpotentials usually vary within a linear range under normal battery operating conditions. Therefore, the exponential function can be linearized as shown in Eq. (18). Comparison between the exponential and the linearized function shows that the difference is about 0.02–0.04 V for the overpotential value up to 0.4 V. Particularly, the use of this linear equation in the charge conservation equation eases convergences of all calculations and reduces computational time.

$$j^{\text{Li}} = a_s i_0 \frac{(\alpha_a + \alpha_c)F}{RT} \eta \quad (18)$$

As matter of fact, the time constant of ion concentration is larger than that for electrons, it is assumed that the second term in the conservation of charge Eq. (3) is regarded as constant. Therefore, concentration and temperature at a given time can be used to calculate κ^{eff} and κ_D^{eff} . Hence, the only unknown variables are the phase potentials, so that the equations are linearized and the number of equations to be solved simultaneously is reduced.

3.6. Numerical calculation

3.6.1. Initial and boundary conditions

Numerical calculation requires initial and boundary conditions to initiate and finalize simulations. The three variables calculated from dynamic equations are lithium ion concentration in solid and electrolyte, and cell temperature, while others are obtained from static equations using these three variables.

The boundary condition for the potential of an electrode is:

$$-\sigma_-^{\text{eff}} \frac{\partial \phi_s}{\partial x} \Big|_{x=0} = -\sigma_+^{\text{eff}} \frac{\partial \phi_s}{\partial x} \Big|_{x=L} = \frac{I}{A} \quad \frac{\partial \phi_s}{\partial x} \Big|_{x=\delta_-} = \frac{\partial \phi_s}{\partial x} \Big|_{x=\delta_+} = 0 \quad (19)$$

where the σ^{eff} is the conductivity, ϕ_s is the solid phase potential, $x = 0$, L represents the interface between the electrode and current collector at negative and positive sides, respectively, and $x = \delta_-$, δ_+ represents the interface between the separator and electrode at negative and positive sides, respectively. For a given current density, the potentials outside of the electrolyte boundary are zero as follows:

$$\frac{\partial \phi_e}{\partial x} \Big|_{x=0} = \frac{\partial \phi_e}{\partial x} \Big|_{x=L} = 0 \quad (20)$$

The initial conditions of various variables are determined from the initial lithium ion concentration in the electrodes. The concentration is expressed as a function of SOC, as follows:

$$c_{s-} = \left(\text{stoi}_0^- + (\text{stoi}_{100}^- - \text{stoi}_0^-) \times \text{SOC} \right) \cdot c_{s-,\text{max}} \quad (21)$$

$$c_{s+} = \left(\text{stoi}_0^+ + (\text{stoi}_{100}^+ - \text{stoi}_0^+) \times \text{SOC} \right) \cdot c_{s+,\text{max}}$$

The concentration of lithium ions inside the particles is spherically symmetric with no generation within, so the gradient of lithium ion concentration at the inner boundary is zero. The outer boundary of electrode particles is determined by the rate of the reaction taking place.

$$r^2 \frac{\partial c_s}{\partial r} \Big|_{r=0} = 0 \quad (22)$$

$$-D_s \frac{\partial c_s}{\partial r} \Big|_{r=R_s} = \frac{j^{\text{Li}}}{a_s F}$$

Since there is no electrolyte flow prior to current flow through the battery, the change in electrolyte concentration at the boundaries is shown below to equal zero.

$$\frac{\partial c_e}{\partial x} \Big|_{x=0} = \frac{\partial c_e}{\partial x} \Big|_{x=L} = 0 \quad (23)$$

The initial cell temperature is set to an ambient temperature. At a low current, heat transfer between the environment and the cell is regarded as negligible. At the boundary,

$$-k \frac{\partial T}{\partial x} = h \cdot (T - T_a) \quad (24)$$

where k is the thermal conductivity of the outer casing, h is the overall convective heat transfer coefficient, T_a is the ambient temperature, and T is the temperature in the cell.

3.6.2. Numerical method

The micro cell is discretized into one hundred grids through the plane. The negative and positive electrodes are meshed with 45 and 34 grids, respectively, because of different thickness of the electrodes. As a result, 179 discrete equations are obtained for the Eqs. (3) and (4) in order to calculate potentials. As potentials and concentrations near both interfaces between electrode areas and separator change drastically, the size of grids at the interfaces should be small enough to minimize the numerical errors. In addition, the small grid is generated at the outer boundary of spheres.

All of equations are converted into discrete forms, coded using MATLAB and solved for the solid phase potentials at the electrodes and the electrolyte phase potential across the cell. For calculations, a finite differential method with an implicit scheme is employed to get converged fast.

The resulting phase and equilibrium potentials are used to calculate overpotential at each section across the cell, which allows for calculation the reaction rate, j^{Li} , using the Butler–Volmer equation. The reaction rate will be inputted to mass balance Eqs. (6) and (7) to determine the change in concentration at each time step. Similar to the method used for the calculation of the reaction rate, an equation for each segment or grid of the battery cell is derived. While the initial values are known, the lithium ion concentration as a function of the change in time provides the variables for the equation.

In fact, electric field in both of electrodes and electrolyte responses faster than that of ion transports when charged and discharged. Therefore, it is assumed that the potentials, ϕ_s and ϕ_e are constant during each time step and calculated just in one subroutine. Conversely, ion transport is dynamically calculated in another subroutine using the mass balance equations for ion concentrations c_s and c_e . The discretized equations can be numerically solved by implicit or explicit method. The major drawback of the implicit method is the difficulty in coding in compared with the explicit one that is less accurate and stable. The code developed is based on the implicit method. The dynamic equation above has

a general form $dc/dt = f(c, \phi)$, where $c = \begin{pmatrix} c_e \\ c_s \end{pmatrix}$ and $\phi = \begin{pmatrix} \phi_e \\ \phi_s \end{pmatrix}$. The potential can be solved from the static Eqs. (3) and (4). Even though both explicit and implicit method assume that the function, f , during two time steps is constant, the explicit method explicitly calculates the function using c and ϕ from the previous time step, while the implicit method considers c and ϕ to be the values of potentials and concentrations in the following time step and calculate them by solving a matrix about c . For calculation of the potential, ϕ , at the following time step, change of concentration for the time step, Δc , instead of c is calculated at a c_0 at the previous time point, which results in the potential ϕ as follows;

$$\phi = \phi_0 + A \cdot \Delta c_e + B \cdot \Delta c_{s,e} \quad (25)$$

where the ϕ_0 is the potential at previous time step, and A and B are coefficient matrices that include the linearized relationship between ϕ and Δc .

4. Static and dynamic analysis and validation of a micro cell

4.1. Potential and overpotential

Standard potentials are determined by the type of chemical compounds used for the electrodes and are a function of the stoichiometric numbers of the chemical compound and SOC. The terminal voltage for a given electrode can be calculated based on the standard potentials. When a battery is charged and discharged, two reversible half reactions occur that cause the potential losses (Overpotentials). The overpotentials of a cell at two different SOCs (50% and 80%) are shown in Fig. 3 under assumption that the OCV at a specified SOC is constant. The concentration overpotential, $\Delta\phi_e$, is the potential difference in the electrolyte phase caused by the concentration of the reactants. In addition, the ohmic and the concentration overpotential are dependent upon the geometry and tend to increase when the film layers become thicker. Conversely, the activation overpotential was not “cumulative” through the plane of the battery film, so that the value is relatively small. The ideal cell voltage in each figure is constant, but varies as a function of SOC.

The Fig. 4 (a) shows the potential of a micro cell, where the x coordinate is a dimensionless number of meshed grids along through-the-plane. The range of the grid for $0 < x < 45$, $46 < x < 67$, $68 < x < 100$ corresponds to the anode, the separator, and the cathode, respectively. We assumed that the potential of the electrolyte at $x = 0$ is the ground potential, so that the potential of the anode and the cathode is about 0.1 V and 3.6 V, respectively. The zoomed-in potentials in the anode are shown in Fig. 4 (b). The difference between the equilibrium potential, U , and the solid

potential is relatively small and varies from $x = 0$ to $x = L$. In fact, the activation overpotential is the difference between the potential in solid, electrolyte, and equilibrium potentials, as shown in Eq. (17).

Fig. 4 (c) shows the cathode and corresponding equilibrium potential and overpotential. The overpotential at the cathode always has an opposite sign when compared to the anode, and in each electrode it can be either positive or negative depending on whether the cell is charging or discharging. In this case, the cell is obviously discharging because the overpotential at the anode is positive, which means the current is flowing from the negative electrode to the electrolyte then to the positive electrode. Fig. 4 (d) shows the corresponding overpotential. Fig. 5

4.2. Current distribution

When a battery is charged or discharged, chemical reactions take place at the interface between the electrodes and electrolyte. As a result, electrons and ions are separated at the cathode. The electrons and ions are transported through an external circuit and the electrolyte, respectively, to anode and combine again there to complete the total reaction. The current in the electrodes is composed of electron current and ion current because of the porosity, while only ion current can go through the separator. The gradient of ion currents is the current density, j^{Li} , whose slope indicates the direction of the current (i.e. positive slope implies that the current flows from solid to electrolyte).

4.3. Concentration of lithium ions

Concentration of lithium ions in solids and electrolyte is the key factor that affects physical variables and states of the battery like SOC, conductivities, and exchange current density. Since the concentration in the solid is not uniformly distributed, only the lithium ion concentration in the electrodes at the outer boundary is shown in Fig. 6, which determines the maximum discharge or charge rate at a moment.

Responses of a high discharging current rate (10C rate) on concentration and current density are shown in Fig. 7. The current density shows a highest value in the electrode at the point of contact with the separator. It decays with time because the migration of ions in both the electrolyte and the electrodes mitigates the difference of reaction rates. It takes several minutes for ion concentration to be uniformly distributed.

In Fig. 8, $r = 0$ represents the center of the electrode particles, while $r = 1$ is the outer boundary of the electrode particles. The geometry of electrodes along with material properties like thickness and porosity result in different concentrations, for example at $L = 0$ and $L = 1$. The magnitudes of concentrations at the boundaries of the separators on the negative electrode are different from that on the positive electrode because of the high conductivity.

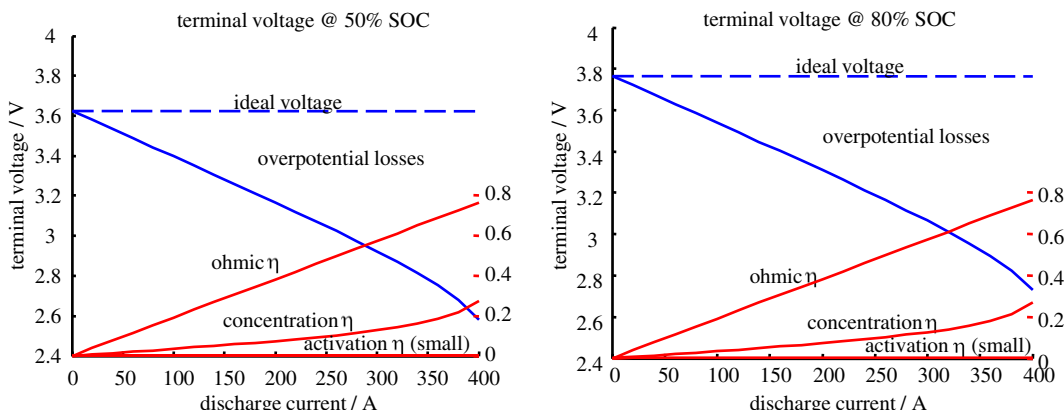


Fig. 3. Overpotentials of micro cell as a function of discharging current at different SOC.

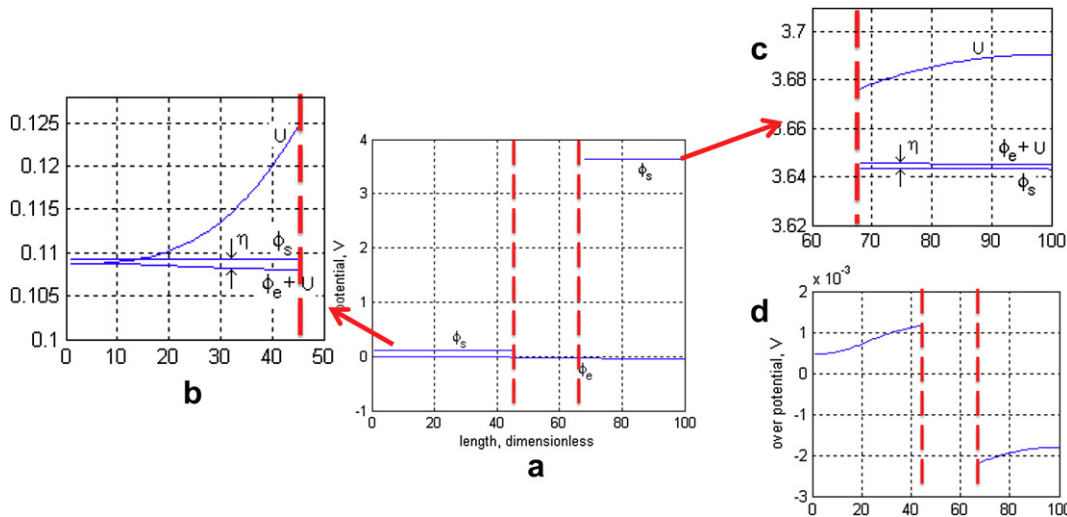


Fig. 4. Potential and overpotential in a micro cell.

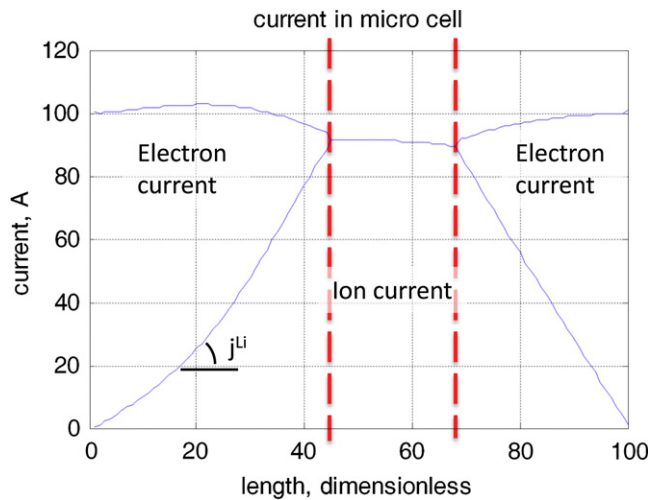


Fig. 5. Current distribution of micro cell.

4.4. Discharging and charging behavior along with validation

Simulation and experiment results of discharging characteristics of a pouch cell are compared in Fig. 9, where the terminal voltages at different current rates are plotted as a function of time. The pouch cell used for the experiments has a capacity of 15.7 A h and its dimensions of the active area are 149.2 mm by 197 mm. When

a discharging current is applied, the terminal voltage drops instantaneously because of ohmic resistances present in the cell. Then, the voltage drops linearly because of the change of the OCV induced by the change of SOC. At the end of each discharge, the experimental shows that the change of the OCV becomes large and as a result the voltage drops drastically. In addition, it should be noted that all of the charges discharged is a function of the current rate. For example, when discharged at 1C, 93% of the maximum capacity is released, while 85% of capacity is released when discharged at 10C.

Generally, charging a cell is carried out by two modes, a constant current mode (CC mode) and a constant voltage mode (CV mode). Transition from one mode to another is simply implemented by changing the boundary condition of the solid conductive Eq. (4). The boundary conditions for the two modes are as follows:

$$\begin{cases} \sum j^{Li} = 0 \\ \phi_{s+} - \phi_{s-} = V_{micro} \end{cases} \quad (26)$$

$$\begin{cases} \sum j^{Li} = 0 \\ \sum j^{Li} = I_{micro}/\Delta L \end{cases} \quad (27)$$

The cell is firstly charged with the CC mode until the terminal voltage reaches 4.2 V and then a constant terminal voltage is applied until the cell is completely charged. While CV charging, the current decays slowly. Simulation and experiment results are compared in Fig. 10, where four different current rates of 20 A, 40 A, 60 A and 80 A are applied.

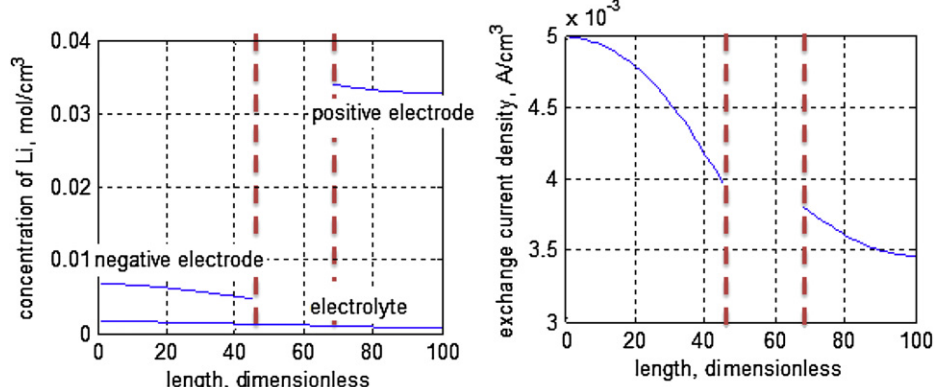


Fig. 6. Lithium ion concentrations and exchange current density in micro cell.

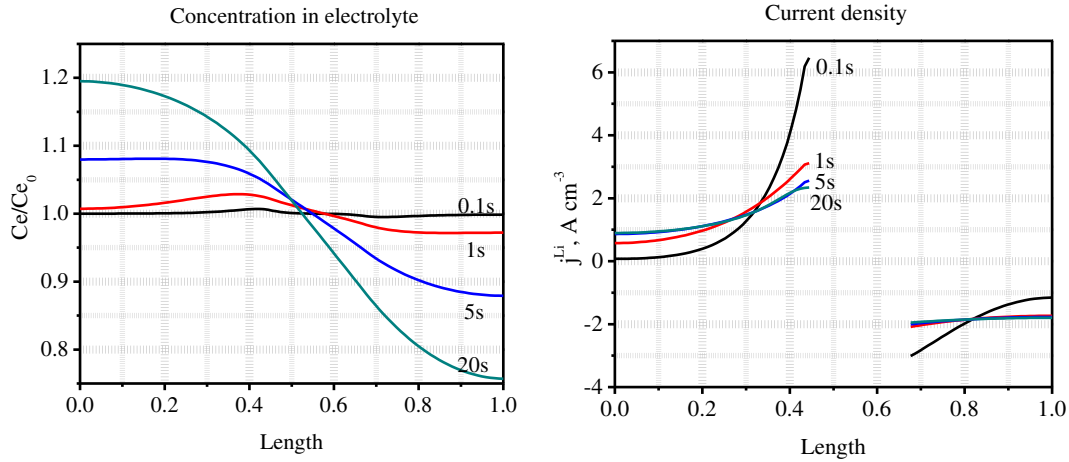


Fig. 7. Unsteady behaviors of concentration and current at 10C discharging.

Comparison of discharging and charging characteristics at the different C rates shows that the model developed can predict the performances.

5. Modeling of a pouch type single cell

Micro cells are connected in parallel by the current collectors that provide a current pathway to the terminal tabs. For each of the current collectors, the potential field is described using Ohm's law:

$$\begin{aligned} \sigma_{cc-} \left(\frac{\partial^2 \phi_{cc-}}{\partial x^2} + \frac{\partial^2 \phi_{cc-}}{\partial y^2} \right) - \frac{I_{\text{micro}}}{l_{cc-}} &= 0 \\ \sigma_{cc+} \left(\frac{\partial^2 \phi_{cc+}}{\partial x^2} + \frac{\partial^2 \phi_{cc+}}{\partial y^2} \right) + \frac{I_{\text{micro}}}{l_{cc+}} &= 0 \end{aligned} \quad (28)$$

where σ_- and σ_+ are the conductivity of aluminum and copper, respectively, ϕ_{cc-} and ϕ_{cc+} are the potentials on two current

collectors, I_{micro} is the current for the micro cells with units of A cm^{-2} , and l_{cc-} and l_{cc+} are the thickness of the current collectors.

Since the cell is made of identical multiple layers of current collectors, it is assumed that the collectors have the same boundary conditions as the load profile at the terminal tabs. I_{micro} that is given by derivatives of the potential field ϕ_{cc} on both current collectors, as described in Eq. (28). On the other hand, the relationship between I_{micro} and the voltage of the corresponding micro cell, $V_{\text{micro}} = \phi_{cc+} - \phi_{cc-}$, should satisfy the nonlinear dynamic micro cell equations, so that all of the micro cells can be coupled to each other.

The simulation results reveal that the I_{micro} is asymmetrically distributed because of the different conductivity of the two current collectors, even though the terminal tabs are symmetrically located. Responses are calculated at 1 s after a 100 A discharging current is applied where the initial temperature is 300 K and the initial SOC is 50%.

The potential distributions on both current collectors are shown in Fig. 11 and Fig. 12. At the positive current collector, the potential near the current tab decreases when the battery is discharging and

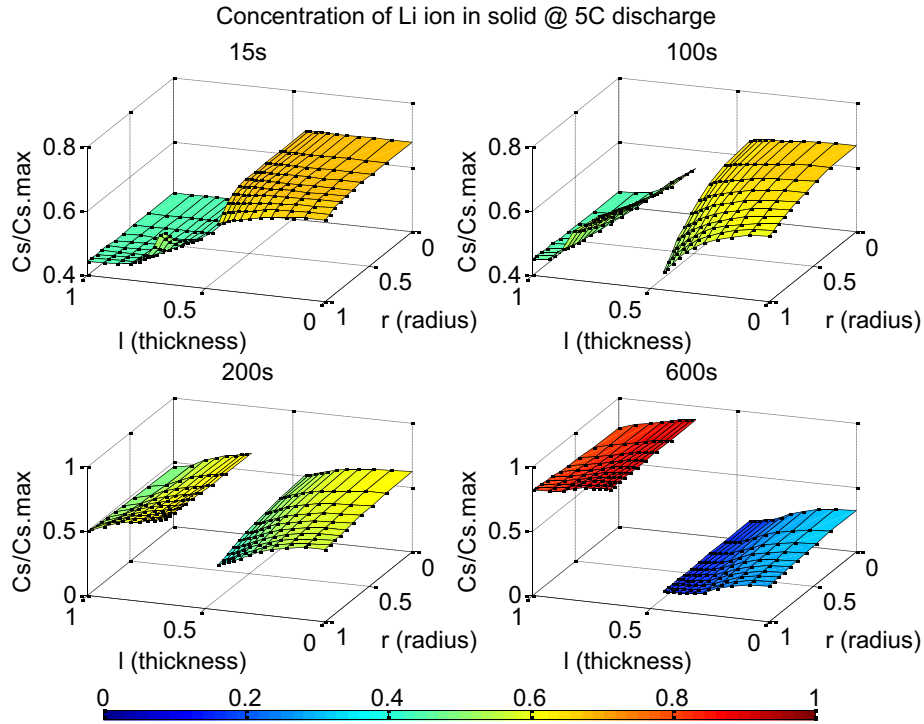


Fig. 8. Response of ion concentration in electrodes.

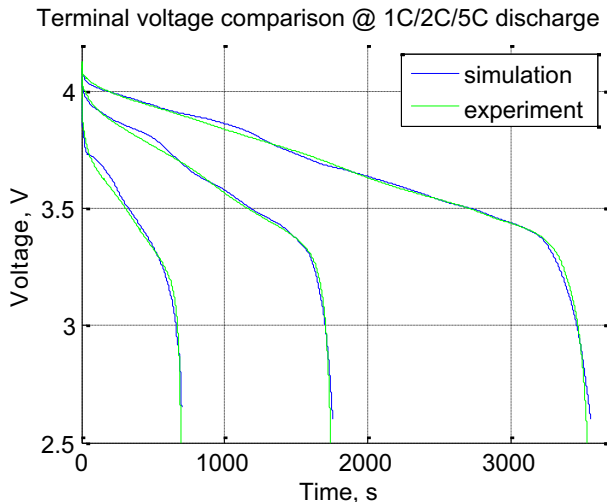


Fig. 9. Discharge characteristics at different current rates (Ambient Temperature = 294 K and SOC = 100%).

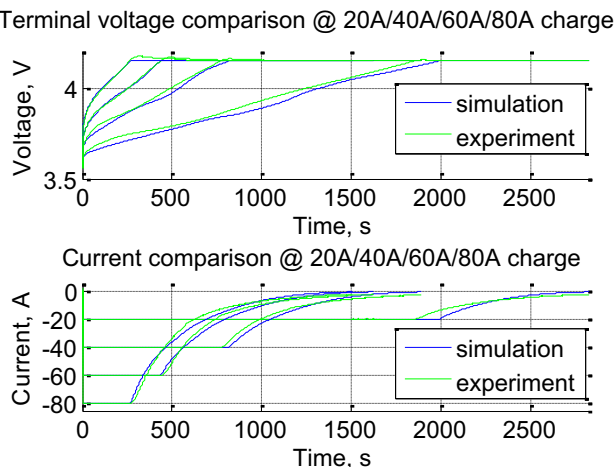


Fig. 10. Charge characteristics at different rates in CC and CV mode.

increases when charging. For each grid, the potential difference between the two current collectors is the potential of micro cell, so the micro cells near the two current tabs show highest overpotential than other locations because of a high reaction rate near the tabs.

Due to the non-uniform potential distribution on both current collectors, the voltages of micro cells are not identical and consequently the reaction rates of micro cells are different from each other. The reaction rate of micro cells determined by the current flow through the micro cells per unit area with an X–Y cross-section is shown in Fig. 13. The reaction rate near terminal tab is

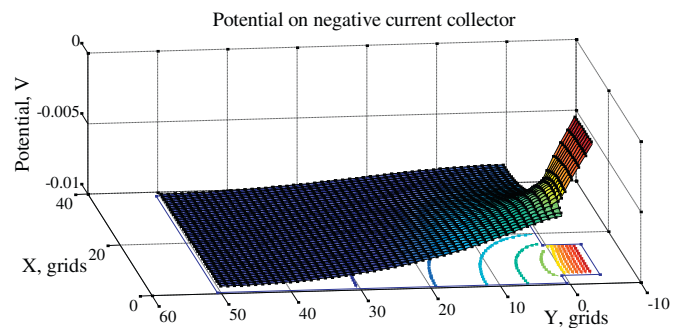


Fig. 12. Potential distributions on negative current collector when discharged.

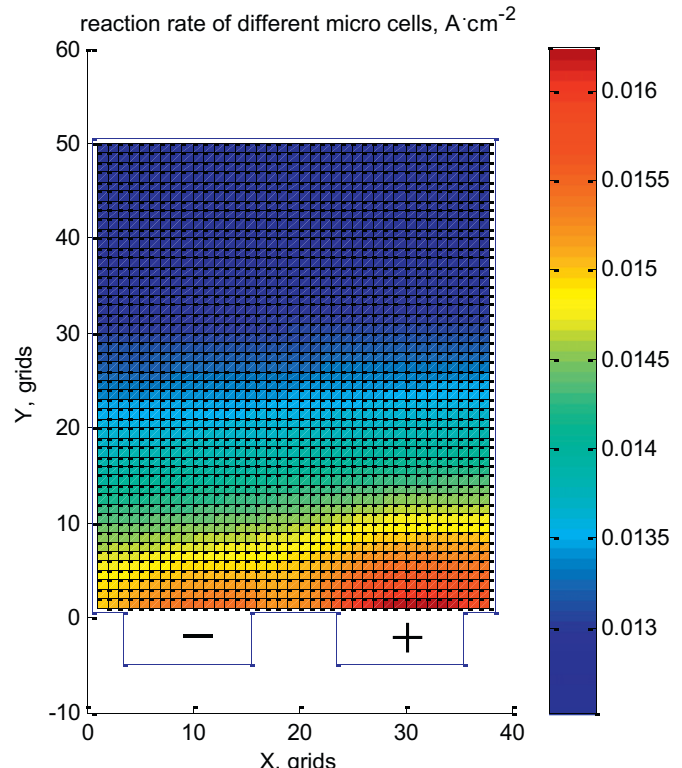


Fig. 13. Initial reaction rates of different micro cells.

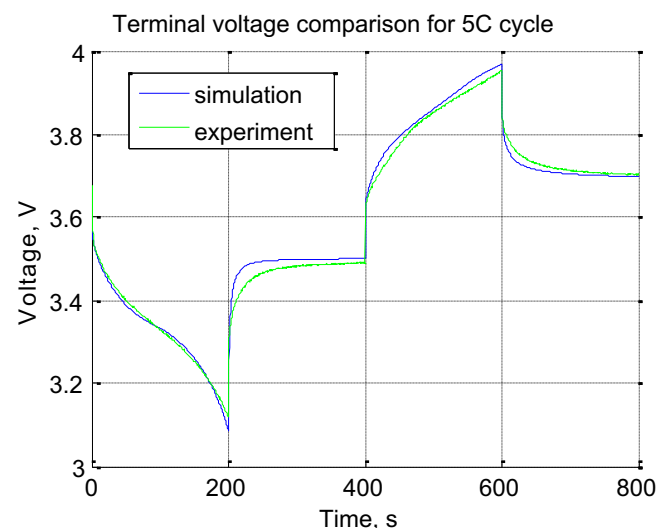


Fig. 14. Voltage response at a single cycle with 5C charging and discharging rate.

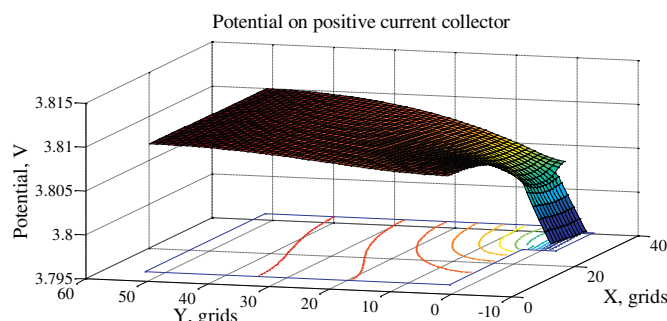


Fig. 11. Potential distributions on positive current collector when discharged.

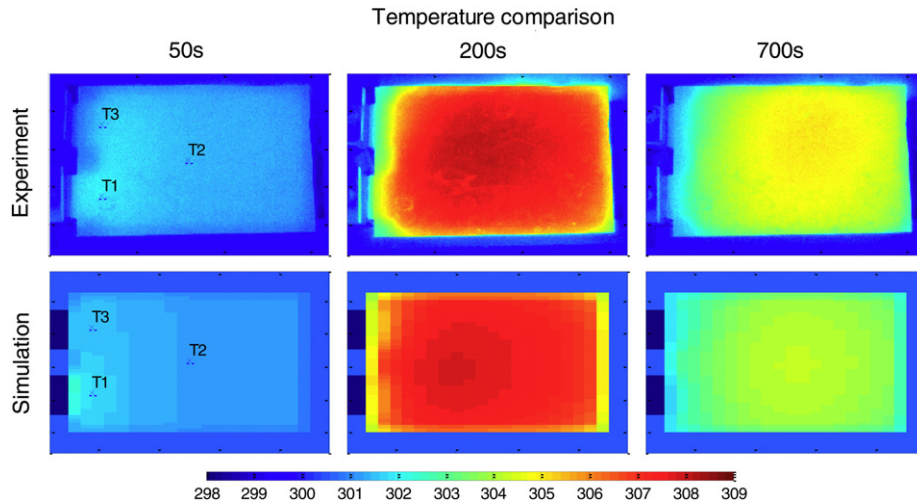


Fig. 15. Temperature distribution of the cell.

higher than that in other area at the beginning. As a result, the SOC of the region is low for a period of time. Since the low SOC leads to a low equilibrium potential, the overpotential decreases if the terminal voltage remains the same as before and consequently the reaction rate get decreased. The results show that the reaction rate near the positive tab is the highest, 20% greater than the lowest grid at the given operating condition.

5.1. Dynamic analysis

In order to assess dynamic responses of the model, an operating condition for a single cycle is defined with initial SOC of 41% and discharge current rate is 5C for 200 s, rest 200 s, charge at 5C current for 200 s then rest 200 s. Comparison of simulation and experiment voltage response is shown in Fig. 14.

In addition, temperature distribution between experiment and simulation is compared in Fig. 15, where the temperature of the cell is captured using IR camera. The temperature distribution in the cell is asymmetric because of the different conductivities of two current collectors. Temperature rise around the positive tab is higher than that in the negative tab. In addition, more heat is generated during discharge process because of exothermic reactions. The temperature increase during discharging is always

greater than that of charging at a given current rate. The calculation for individual heat source terms shows a distribution of Joule heating in electrolyte (38%), heat of mixing (24%), heat caused by activation losses (16%), change of entropy (10%), Joule heating at SEI (8%), Joule heating at the current collectors (4%) and others.

In addition, temperature of three locations of the cell are measured and compared with that of the simulation as shown in Fig. 16. The simulation results follow the experiment results with some time delay and errors that are possibly affected by the heat transfer between the cell and air flow in a thermal chamber.

6. Conclusion

We developed a high resolution quasi-three dimensional model for a pouch type of lithium polymer cell with a chemistry of $\text{LiMn}_2\text{O}_4/\text{Carbon}$ for electrodes. The model is constructed using a one dimensional micro cell based on electrochemical and thermal principles and experimentally validated against static and dynamic performance of a cell.

Analysis shows following interesting findings:

1. Due to different conductivities of the two current collectors, asymmetrical distribution of the current and voltage field is observed. The asymmetric current field causes non-uniform heat generation rates on the current collectors. Particularly, more heat is generated on the current collector located near the terminal tabs. Similarly, the asymmetric voltage field affects the reaction rates of micro cells, so heat generation rates and the associated DOD are different dependent upon location.
2. Contribution of individual heat source terms are analyzed, where the heat caused by Joule heating in electrolyte and heat of mixing are the major parts at the 5 C rate.

The model developed is capable of representing not only current and voltage at the terminal tabs of a single cell but also distribution of ion concentrations, potentials, internal currents, and temperature when a battery is charged or discharged. Future work includes measurement of the individual heat source terms and validation of the model for other ambient temperature ranges.

Acknowledgement

This project is funded by General Motor Corporation. The authors do appreciate the technical discussions and financial support.

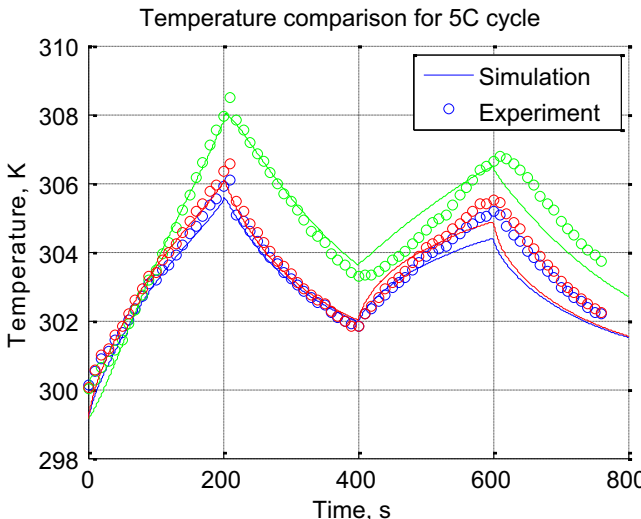


Fig. 16. Temperature comparison at three locations.

Appendix. parameters

	Parameter	Negative electrode	Separator	Positive electrode	unit
Design specifications (geometry and volume fractions)	Thickness, δ	$50*10^{-4}$	$25.4*10^{-4}$	$36.4*10^{-4}$	cm
	Particle radius, R_s	$1*10^{-4}$		$1*10^{-4}$	cm
	Active material volume fraction, ϵ_s	0.58		0.5	
	Polymer phase volume fraction, ϵ_p	0.048	0.5	0.11	
	Conductive filler volume fraction, ϵ_f	0.04		0.06	
Solid and electrolyte phase Li^+ concentration	Porosity, ϵ_e	0.332	0.5	0.33	
	Maximum solid phase concentration, $c_{s,\max}$	$42.2*10^{-3}$		$74.9*10^{-3}$	mol cm^{-3}
	Stoichiometry at 0% SOC: $x_{0\%}, y_{0\%}$	0.123		0.939	
Kinetic and transport properties	Stoichiometry at 100% SOC: $x_{100\%}, y_{100\%}$	0.685		0.434	
	Average electrolyte concentration, c_e	$1.2*10^{-3}$	$1.2*10^{-3}$	$1.2*10^{-3}$	mol cm^{-3}
	Exchange current density coefficient, k_{i0}	13.2		6.79	A cm^{-2}
	Charge-transfer coefficient, α_a, α_c	0.5, 0.5		0.5, 0.5	
	Solid phase Li diffusion coefficient, D_s	$1.0*10^{-11}$		$1.85*10^{-11}$	$\text{cm}^2 \text{s}^{-1}$
	Solid phase conductivity, σ	1		0.1	S cm^{-1}
	Electrolyte phase Li^+ diffusion coefficient, D_e	$2.6*10^{-6}$	$2.6*10^{-6}$	$2.6*10^{-6}$	$\text{cm}^2 \text{s}^{-1}$
	Bruggeman's porosity exponent, p	1.5	1.5	1.5	
	Electrolyte phase ionic conductivity, κ	$7.9c_e$ $\exp(-13472c_e^{1.4})$		$7.9c_e$ $\exp(-13472c_e^{1.4})$	S cm^{-1}
	Li^+ transference number, t_{+}^0	0.363	0.363	0.363	

References

- [1] M. Doyle, T. Fuller, J. Newman, J. Electrochem. Soc. 140 (1993) 1526–1533.
- [2] T.F. Fuller, M. Doyle, J. Newman, J. Electrochem. Soc. 141 (1994) 1–10.
- [3] V. Srinivasan, J. Newman, J. Electrochem. Soc. 151 (2004) A1517–A1529.
- [4] P. Albertus, J. Christensen, J. Newman, J. Electrochem. Soc. 156 (2009) A606–A618.
- [5] M. Doyle, T. Fuller, J. Newman, Electrochimica Acta 39 (1994) 2073–2081.
- [6] S. Stewart, J. Newman, Electrochem. Soc. 155 (2008) A458–A463.
- [7] S. Stewart, J. Newman, Electrochem. Soc. 155 (2008) F13–F16.
- [8] G. Nagarajan, J. Zee, J. Electrochem. Soc. 145 (1998) 771–779.
- [9] L. Song, J. Evan, J. Electrochem. Soc. 147 (2000) 2086–2095.
- [10] C. Chiasseroni, R. Rao, IEEE Journal on Selected Areas in Communications 19 (2001) 1235–1245.
- [11] R. Darling, J. Newman, J. Electrochem. Soc. 145 (1998) 990–998.
- [12] T. Fuller, M. Doyle, J. Newman, J. Electrochem. Soc. 141 (1994) 982–990.
- [13] K. Smith, C.Y. Wang, J. Power Sources 161 (2006) 628–639.
- [14] D. Rakhmatov, IEEE Transactions on Very Large Scale Integration (VLSI) Systems 11 (2003) 1019–1030.
- [15] Y. Chen, J. Evans, J. Electrochem. Soc. 140 (1993) 1833–1838.
- [16] M. Doyle, Y. Fuentes, J. Electrochem. Soc. 150 (2003) A706–A713.
- [17] K. Smith, C.Y. Wang, J. Power Sources 160 (2006) 662–673.
- [18] V. Srinivasan, C.Y. Wang, Electrochim. Soc. 150 (2003) A98–A106.
- [19] E. Peled, Electrochimica Acta 40 (1995) 2197–2204.